International Journal of Computer Science and Information Technology
ISSN: 3005-9682 (Print), ISSN: 3005-7140 (Online) | Volume 2, Number 1, Year 2024
DOI: https://doi.org/10.62051/ijcsit.v2n1.55
Journal homepage: https://wepub.org/index.php/IJCSIT/index

Core Image Lithology Identification

Liying Yang

Resource and Environmental College, Henan Polytechnic University, Jiaozuo, Henan 454000, China

ABSTRACT

Core is a part of subsurface rock formations, and rock classification can be achieved by analyzing lithological characteristics such as color, texture, or shape. This is an essential step in oil and gas exploration. In the field of geology, core image analysis is a method for studying the micro-features of rocks, utilizing color and texture characteristics from core images for lithology identification. This paper establishes three models: one utilizing color moments for neural network training, another using gray-level co-occurrence matrix for neural network training, and a third employing a fusion of color moments and gray-level co-occurrence matrix for neural network training. The results from the three models are compared to assess the experimental accuracy. The findings indicate that the multi-feature fusion approach demonstrates higher precision in core image lithology identification.

KEYWORDS

Core image; Color moments; Gray-level co-occurrence matrix; Multi-feature fusion; Lithology.

1. INTRODUCTION

Core is an extremely important physical geological material in geological engineering research, including mineral extraction and petroleum exploration . Core provides intuitive information in oil and gas exploration and development and is a frequently utilized physical material. Data for petroleum geological analysis and geophysical exploration parameters are often derived from core samples. Quantitative analysis and processing of core image data serve as a primary basis for in-depth exploration and development of petroleum geology .Sedimentary rocks are formed through the processes of sediment accumulation and diagenesis during crustal movement, exhibiting complex compositions, structures, and relationships. Currently, there is no unified classification standard due to this complexity. Therefore, this study refers to contemporary and popular classification ideas mentioned in mainstream textbooks to categorize rock types in the research samples [3-4].Various researchers have contributed to the field. Meng X , through the identification of sedimentary structural features in cores, determined the depositional facies of the Paleogene Shahejie Formation in the Dongying Sag's southern slope. Ren Yili proposed automated lithology identification based on core images, lithology intelligent identification based on well logging curves, and lithology intelligent identification based on transfer learning, achieving tangible results. Bai Lin constructed a deep learning model for rock identification based on convolutional neural networks, achieving a recognition accuracy of 63%. Chen Hao applied mathematical morphology image processing techniques to the quantitative study of mudstone laminations in core photos, effectively quantifying the qualitative research results of mudstone laminations. Zhu Qiangjun , through fuzzy enhancement of core images, employed a median filter for smooth processing, extracting stratigraphic features from core images. Zhang B utilized transfer learning and neural networks for automated core image representation and identification, aiding in accurate real-time identification of sedimentary structures and reservoir quality prediction.Other studies include Li Jiahang , who established characterization

parameters for the development degree of shale laminations based on transitional marine-continental facies; Borazjani O , who developed intelligent systems for identifying carbonate texture and pore space features from thin section images; Peng Yue , who used image recognition technology to define dimensionless crack development indices, quantitatively evaluating the degree of crack development in the single-well reservoir control body; Hu Bo , who, based on high-precision digital core images, developed an adaptive pore recognition and extraction method, a pore segmentation method based on image morphology algorithms, and a method for calculating pore structure feature parameters, achieving quantitative characterization of micro-pore structures in tight sandstones based on scanned images; Yu Xiaolu , who employed convolutional neural networks for the processing of carbonate thin section images, identifying and analyzing features such as biological species and quantities; Qin Rong , who used X-ray fluorescence (XRF) core scanning for studying laminations in other lake sediments.David Wettergreen applied shape, texture, and pattern features of image content to detect and segment rocks in surface images of Mars. Zhang Ye established a deep learning transfer model based on Inception-v3 for effective recognition of three types of rocks: granite, breccia, and conglomerate. Liu Liting developed a rock image classification model using deep neural networks. Song Wenguang proposed an intelligent lithology identification method based on generative adversarial networks, achieving intelligent classification of sedimentary rock lithology. Zhang Zhongya designed a lightweight convolutional neural network model to identify components in sandstone thin section images. Ma Zedong proposed a multi-scale lithology recognition method that performs well in identifying rock lithology.

The inherent complexity of core structures, such as particle roundness, grain size, sorting, and mineral composition, changes with the increasing transport distance, adding difficulty to core identification. Therefore, a robust feature set is needed to describe the features of core images, especially the most prominent texture features. From the current research status, there are numerous feature algorithms for core image lithology identification, whether based on pixel-level features or object-level texture features, that can effectively identify core images. However, most feature sets are proposed for a specific type, and there is limited literature on multi-feature extraction algorithms for core images. Therefore, how to analyze sedimentary structures in cores based on multi-feature fusion is an essential aspect.

2. CORE IMAGE PREPROCESSING

2.1. Establishment of Core Image Dataset

In the analysis of lithology in core images, common sedimentary rocks such as sandstone, conglomerate, fine sandstone, mudstone, and gravel are studied, and the main characteristics of these sedimentary rocks are shown in Table 1. To prevent overfitting and enhance the accuracy of the model during neural network training, it is essential to rely on an ample dataset. Given the limited availability of core samples, data augmentation is employed to address the issue of insufficient data. The data augmentation strategy encompasses various transformations such as cropping, rotation, scaling, and mirroring, aiming to enrich the diversity of the training set. This enables the neural network to better learn and generalize the features of core samples.

A dataset containing a large number of rock samples was successfully constructed through systematic collection, screening, and classification of core images. During the experimental phase, a diverse dataset was created by randomly combining different rock types such as sandstone, conglomerate, fine sandstone, mudstone, and gravel for classification. In the process of dataset partitioning, following an 8:2 ratio principle, the dataset was divided into a training set and a testing set. This ratio, validated through experiments, was determined to achieve the optimal performance in model training and evaluation. This dataset construction and partitioning method ensures the model's thorough

learning and generalization capabilities across various rock types. Figure 1 shows examples of core samples.

Table 1. Main Characteristics of 5 Types of Sedimentary Rocks

Sedimentary Rock Type	Main Characteristics
Sandstone	Particle diameter between 0.1-2 millimeters, major clastic components include quartz, feldspar, and rock fragments.
Conglomerate	Primarily composed of sandstone particles with varying particle size distribution, considered a composite sandstone. Typically contains gravel stones, with gravel content less than five percent, and conglomerate content exceeding five percent.
Fine Sandstone	Clastic rock composed of particles with diameters between 0.01-0.1 millimeters. If fine sandstone contains a significant amount of sand and clay, it can be named following the three-level composite naming principle.
Mudstone	Particles smaller than 0.0625 millimeters, deposited but not fully consolidated, and lacks bedding in clastic rocks.
Gravel	Coarse particles with diameters above 2 millimeters, ranging up to several centimeters. Particles can be round, oval, or angular, and the majority are rock fragments.

(a)Mudstone(b)FineSandstone(c)Sandstone(d)Conglomerate(e)Gravel(f)Mud-rich Fine Sandstone

Figure 1. Core Sample Images

Table 2. Distribution of Core Image Data

Rock Type	Number of Samples	Training Set per Image	Testing Set per Image
Mudstone	130	104	26
Fine Sandstone	105	84	21
Sandstone	125	100	25
Conglomerate	135	108	27
Gravel	135	108	27
Mud-rich Fine Sandstone	105	84	21

Before proceeding with the training of the neural network model, it is crucial to rigorously preprocess the data to ensure uniform formatting and size for core images. Given the variations in sizes among the core images in the dataset, normalization of the core image dimensions is necessary to enhance the stability and performance of the model. Specifically, out of the original dataset comprising 735 core images, a standard size of 350×200 pixels was employed for scaling purposes.Concerning dataset partitioning, the core images were divided into two parts, following an 8:2 ratio for the training and testing sets. Out of the 735 core images, 588 were allocated for training the model, while the remaining 147 core images were reserved for validating the model's accuracy. Table 2 provides a

detailed breakdown of the distribution of core images across different sections of the dataset. This series of preprocessing steps and dataset partitioning aims to ensure that the neural network model benefits from standardized input data during both the training and evaluation phases.

2.2. Denoising of Core Images

When photographing core bedding, various factors such as human intervention, equipment limitations, or environmental conditions can introduce noise to core photos. Therefore, during sample selection, efforts were made to ensure similar conditions among multiple images, minimizing errors caused by external factors and manual operations. In order to mitigate the impact of noise on core image recognition, salt-and-pepper noise was introduced after converting the core images to grayscale (Figure 2). The purpose of this experimental design was to simulate potential noise interference present in real-world environments and comprehensively evaluate the applicability of different denoising methods in core image processing. The introduction of salt-and-pepper noise aims to assess the impact of various denoising methods on image quality and the recognition of core structures. Through this study, we gain a comprehensive understanding of the performance of different denoising methods in the presence of noise, providing a scientific basis for image processing in the field of petrology.

(a) Original Core Image (b) Grayscale Image

Figure 2. Grayscaling of Core Images

Median filtering is a non-linear signal smoothing technique based on the theory of order statistics. It effectively suppresses noise by setting the grayscale value of each pixel to the median value of all pixel values within a certain neighborhood window. This method eliminates the interference from isolated points and lines, reducing high-frequency components in the Fourier space. By replacing the center grayscale value with the median, it ensures the step and slope functions remain unchanged, effectively preserving image edge information. Additionally, it can remove certain uniformly distributed noise and salt-and-pepper noise.

For one-dimensional median filtering with an odd number of points in the sliding window, the value of the center point in the window is replaced by the median value of all points within the window. If a window length of n (odd number) is applied to a one-dimensional digital sequence, the median filtering involves selecting 2k+1 values from the sequence, where k is the window's radius. The selected values are then sorted by their numerical order, and the median of this data set becomes the output value after filtering. The expression is as follows:

$$Y_i = M_{ed}\{x_{i-k}, \cdots x_{i-1}, x_i, x_{i+1}, \cdots x_{i+k}\} \quad (1)$$

In two-dimensional median filtering, the pixels within a two-dimensional sliding template are sorted based on their pixel values, creating a monotonically increasing (or decreasing) two-dimensional data sequence. The expression is as follows:

$$g(x,y) = M_{ed}\{P(x-k, y-k), \cdots P(x-1, y), P(x,y), \cdots P(x, y+1), P(x+k, y+k)\} \quad (2)$$

where:is the value after median filtering in the window data.

When dealing with core images that have been affected by salt-and-pepper noise, median filtering with different window sizes is applied. The aim is to assess the effectiveness of various median filtering window sizes in removing salt-and-pepper noise, ultimately determining the most suitable median filtering parameters for core images. Through systematic observation and comparison of experimental results, a comprehensive understanding of the denoising performance of median filtering under different window conditions for core images can be obtained. The results are illustrated in Figure 3.

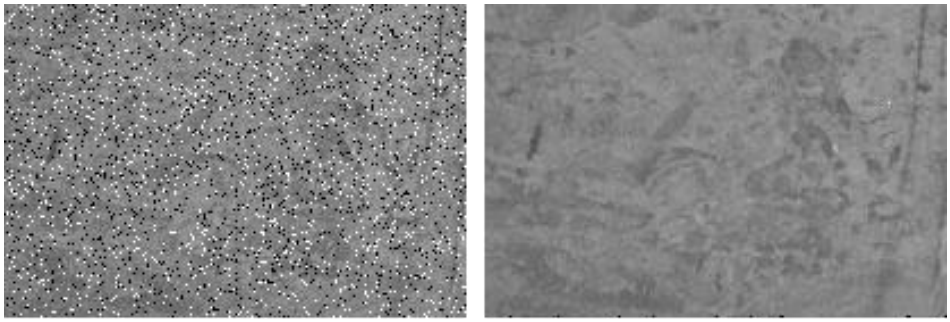

(a)mage with Added Salt-and-Pepper Noise (b)Median Filtering (Kernel Size: 1)

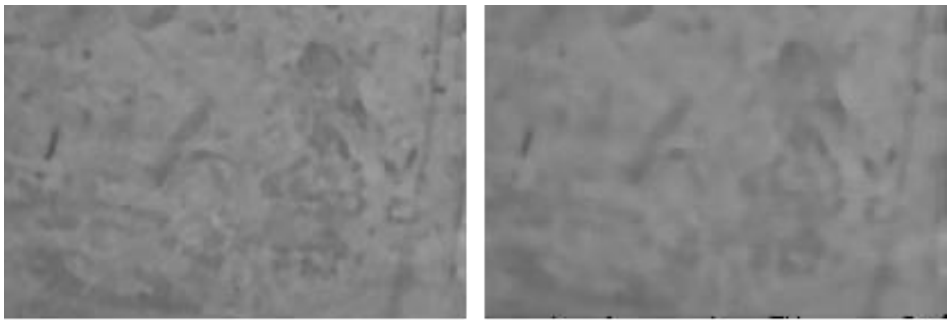

(c)Median Filtering (Kernel Size: 3) (d)Median Filtering (Kernel Size: 5)

Figure 3. Median Filtering Results

Upon observing the results of median filtering, it was noted that with the increase in the size of the median filtering mask, the core image successfully removed salt-and-pepper noise but concurrently lost a significant amount of edge information. Based on the experimentation with different-sized windows for median filtering and mean filtering, a median filter with a kernel size of 1 was selected as the optimal denoising method. Despite its smaller size, this choice effectively balanced denoising and information preservation in core images. Through appropriate denoising, critical edge information in the images was successfully retained. This optimization decision is grounded in a profound understanding of the trade-off between filter size and denoising effectiveness, contributing to enhanced accuracy in core image analysis.

3. NEURAL NETWORK-BASED LITHOLOGY IDENTIFICATION

3.1. Neural Network Principles

In the study of lithology identification in core images, a Multi-Layer Perceptron (MLP) was chosen to construct the model, leveraging its advantages in complex feature learning. By training the deep learning model on the features of core images, efficient and accurate automatic identification of lithology was achieved. This approach, utilizing the non-linear mapping capability of the Multi-Layer Perceptron, allows for the extraction of abstract representations from core images, better capturing the complex features and spatial relationships of lithology. Consequently, this enhances the accuracy and robustness of lithology identification. The principles of MLP can be divided into two main steps:

forward propagation and backward propagation. The MLP network structure is illustrated in Figure 4.

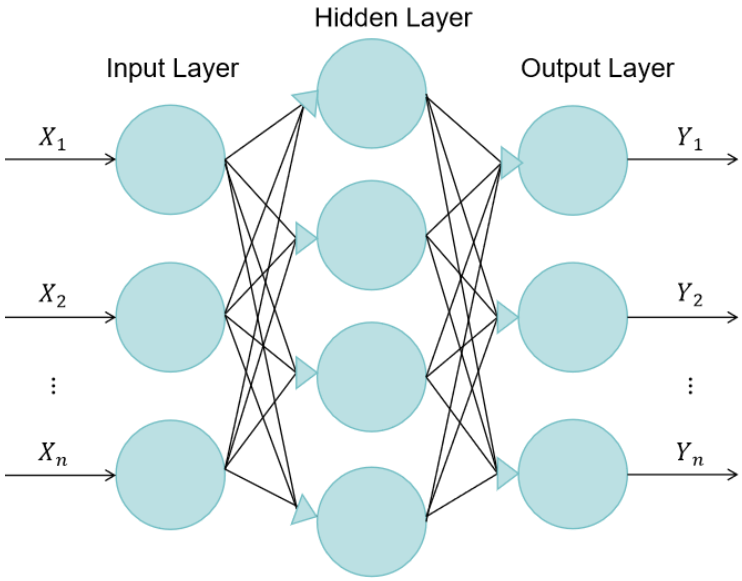

Figure 4. MLP Network Structure

The principle is based on the ReLU (Rectified Linear Unit) function, denoted as r(x). A linear transformation is applied to the input of r(x), represented as r(ax+b), inducing horizontal translation and scaling of the function. Additionally, a linear transformation is applied to the output of r(x), such as c*r(ax+b)+d, resulting in vertical translation and scaling of the function. The flowchart is illustrated in Figure 5.

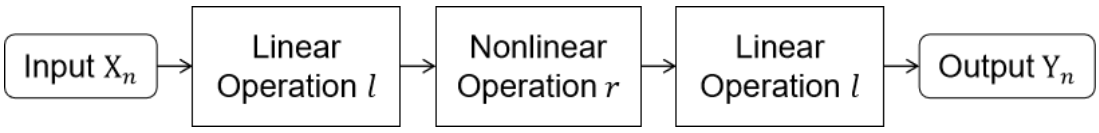

Figure 5. Flowchart of MLP Network Operational Principles

The forward propagation formula is as follows:

$$a^{(l+1)} = g(z^{(l+1)}) \tag{3}$$

$$z^{(l+1)} = W^{(l+1)}a^{(l)} + b^{(l+1)} \tag{4}$$

where: $a^{(l)}$ is the output of the l-th layer, $z^{(l+1)}$ is the input of the l-th layer, $W^{(l+1)}$ is the weight matrix, $b^{(l+1)}$ is the bias vector, $g(\cdot)$ is the activation function.

The objective of backward propagation is to minimize the loss function by adjusting weights and biases. The formula is as follows:

$$\frac{\partial L}{\partial W^{(l+1)}} = \frac{\partial L}{\partial z^{(l+1)}} \cdot \frac{\partial z^{(l+1)}}{\partial W^{(l+1)}} \tag{5}$$

$$\frac{\partial L}{\partial b^{(l+1)}} = \frac{\partial L}{\partial z^{(l+1)}} \cdot \frac{\partial z^{(l+1)}}{\partial b^{(l+1)}} \tag{6}$$

$$\frac{\partial L}{\partial a^{(l)}} = \frac{\partial L}{\partial z^{(l+1)}} \cdot \frac{\partial z^{(l+1)}}{\partial a^{(l)}} \tag{7}$$

where: L is the loss function., $\frac{\partial L}{\partial z^{(l+1)}}$ is the gradient of the loss function with respect to the input of layer $l+1$.

For the rock core image dataset that has undergone lithological classification, a pre-built neural network was employed for model training. During the training process of core images, forward and

backward propagation were iteratively executed multiple times, continuously adjusting the parameters of the neural network to gradually align the model's predictions with the actual labels. This iterative training approach helps optimize the model's performance, enabling it to effectively capture complex features within core images and make accurate predictions in various lithological contexts.

3.2. Color Moment Recognition

When classifying the multiple categories of lithology, especially in the case of clastic rocks, training the neural network using color features and evaluating its accuracy in lithological discrimination is essential. The feature extraction process for lithology utilizes color moments, a mathematical approach that describes the distribution of colors in an image using computed moments. Since colors in the core images of clastic rocks are primarily distributed in lower-order moments, only the first moment (mean), second moment (variance), and third moment (skewness) of color are sufficient to express the color features of the image. The combination of these three moments effectively captures the basic statistical information of color distribution in the image, providing a specific and concise feature representation for subsequent lithology recognition tasks. The color moments in the image only require 9 components, and their formulas are as follows:

$$\mu_i = \frac{1}{N}\sum_{j=1}^{N} p_{i,j} \tag{8}$$

$$\sigma_i = \left(\frac{1}{N}\sum_{j=1}^{N}(p_{i,j} - \mu_i)^2\right)^{\frac{1}{2}} \tag{9}$$

$$s_i = \left(\frac{1}{N}\sum_{j=1}^{N}(p_{i,j} - \mu_i)^3\right)^{\frac{1}{3}} \tag{10}$$

where: i represents the color channel, and N represents the total number of pixels in the image.$p_{i,j}$ represents the pixel value of the j-th pixel in the i-th color channel,μ_i(First Moment) represents the mean value of all pixels in the i-th color channel,σ_i (Second Moment) represents the standard deviation of all pixels in the i-th color channel,s_i(Third Moment)represents the cube root of the skewness of all pixels in the i-th color channel.

In the HSV color space, the feature vector of color moments in the image can be expressed as:

$$V_{color} = [\mu_H, \sigma_H, s_H, \mu_S, \sigma_S, s_S, \mu_V, \sigma_V, s_V] \tag{11}$$

After preprocessing the rock core images in the training set and extracting color features, the values of color moments are obtained. These values serve as data features for training the neural network model. When constructing the neural network model, the input layer consists of the types of data features. In the case of using color moment features, the input layer is set to 9. Figure 6 illustrates the model training process using color moments. The horizontal axis represents the number of training rounds, and the vertical axis represents the training accuracy. The accuracy reflects the average precision of the model. The blue line represents the accuracy on the training set, while the orange line represents the accuracy on the test set. From the graph, it can be observed that the model's accuracy increases with the number of rounds until it plateaus. Finally, training the neural network with color moments achieves an accuracy of approximately 75%.

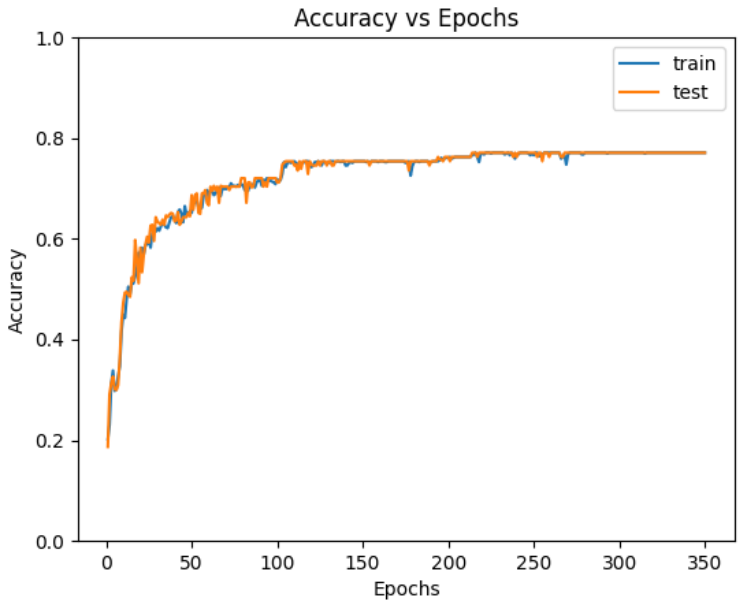

Figure 6. Accuracy with Color Moment Features

3.3. GLCM Recognition

For rock lithology identification, texture features provide an effective method for detecting lithology. The commonly used Gray Level Co-occurrence Matrix (GLCM) method, which measures second-order statistics to quantify texture image features, is employed. There are 14 feature parameters commonly used for texture analysis. Different combinations of matrix generation parameters, such as varying step lengths and image grayscale levels, can yield different co-occurrence matrices. Concurrent studies suggest that five parameters can effectively and consistently describe texture features.

(1) Entropy (ENT):Entropy serves as a measure of information in texture images, describing the non-uniformity and complexity of the image texture. A smaller entropy indicates rough and uneven texture, reaching zero for a texture-free image, while the entropy is maximized for a fully textured image.

$$\mathrm{ENT} = -\sum_{i=1}^{g}\sum_{j=1}^{g} P(i,j,d,\theta) \times \lg P(i,j,d,\theta) \tag{12}$$

(2)Contrast (CON):Describes the depth of grooves in the texture of the rock core; a higher value indicates deeper grooves in the texture elements, resulting in a clearer image. The calculation formula is as follows:

$$\mathrm{CON} = \sum_{i=1}^{g}\sum_{j=1}^{g}[(i-j)^2 \times P^2(i,j,d,\theta)] \tag{13}$$

(3)Energy (Angular Second Moment, ASM):** Measures the uniformity of grayscale variations in the rock core image texture. A higher value indicates finer texture, while a lower value suggests rougher texture. The calculation formula is as follows:

$$\mathrm{ASM} = \sum_{i=1}^{g}\sum_{j=1}^{g} p^2\,(i,j,d,\theta) \tag{14}$$

(4) Inverse Difference Moment (IDM): Represents the regularity of the rock core image texture. A higher value of the inverse difference moment indicates a more regular texture.

$$\mathrm{IDM} = \sum_{i=1}^{g}\sum_{j=1}^{g} P(i,j,d,\theta)/[1+(i-j)^2] \tag{15}$$

(5) Correlation: Describes the similarity of the gray levels between adjacent pixels. The correlation is smaller when the values of elements in the gray-level co-occurrence matrix differ more. The formula for calculation is:

$$\mathrm{CORRLN} = \sum_{i=1}^{g}\sum_{j-1}^{g}\frac{[i\times j\times p(i,j,d,\theta)-u_1\times u_2]}{(d_1\times d_2)} \quad (16)$$

where: μ_1 and μ_2 are the means of the gray-level co-occurrence matrix in rows and columns, respectively.d_1^2 and d_2^2 are the standard deviations of the gray-level co-occurrence matrix in rows and columns, respectively.

$$\mu_1 = \sum_{i=1}^{g} i \sum_{j=1}^{g} p(\mathrm{i,j,d},\theta)$$

$$\mu_2 = \sum_{j=1}^{g} j \sum_{i=1}^{g} p(\mathrm{i,j,d},\theta)$$

$$d_1 = \sqrt{\sum_{i=1}^{g}(i-u_1)^2 \sum_{j=1}^{g} p(\mathrm{i,j,d},\theta)}$$

$$d_2 = \sqrt{\sum_{j=1}^{g}(j-u_1)^2 \sum_{i=1}^{g} p(\mathrm{i,j,d},\theta)}$$

Table 3. Gray-Level Co-occurrence Matrix Feature Values

Sample Category	Angle	Entropy	Contrast	Energy	Inverse Difference Moment	Correlation
Mudstone	0°	0.06524013	77.86890234	0.00425627	0.28563185	0.82911562
	45°	0.0569772	128.24486778	0.0032464	0.226525	0.71845801
	90°	0.05975563	115.47991127	0.00357074	0.24821773	0.7467516
	135°	0.06350061	86.99992217	0.00403233	0.27536587	0.80907472
Siltstone	0°	0.04898714	81.50402441	0.00239974	0.1920198	0.88072035
	45°	0.04826964	68.90184494	0.00232996	0.18366862	0.89826097
	90°	0.0466921	77.42286415	0.00133881	0.15499862	0.84781036
	135°	0.04919141	75.74842647	0.0024198	0.19360705	0.88914368
Sandstone	0°	0.03908914	120.64085203	0.00152796	0.17382129	0.71869624
	45°	0.03678704	146.72697022	0.00135329	0.15130977	0.65146689
	90°	0.03658974	77.42286415	0.00133881	0.15499862	0.84781036
	135°	0.03892282	121.73436358	0.00151499	0.17251176	0.71606732
Conglomeratic Sandstone	0°	0.02114703	140.13876545	0.0004472	0.17139457	0.9090929
	45°	0.01859456	211.30945732	0.00034576	0.1332026	0.86289852
	90°	0.01909262	213.99443061	0.00036453	0.1444918	0.86121009
	135°	0.02109782	132.30799893	0.00044512	0.16879357	0.91417281
Conglomerate	0°	0.01719409	390.21843012	0.00029564	0.09694688	0.752741
	45°	0.01634366	449.38702878	0.00026712	0.08468271	0.7158732
	90°	0.01562033	560.7865965	0.00024399	0.07637276	0.64344797
	135°	0.01734093	360.04647416	0.00030071	0.09920798	0.77185716
Muddy Siltstone	0°	0.03618791	71.38246988	0.00130957	0.16914143	0.91892003
	45°	0.03716481	47.15201824	0.00138122	0.18182485	0.94641999
	90°	0.03316133	147.42403469	0.00109967	0.13650003	0.83262676
	135°	0.03638881	72.27792169	0.00132415	0.17174889	0.91790348

Based on the principle of gray-level co-occurrence matrix, values for five parameters were selected from four directions (0°, 45°,90°, 135°) to extract features from the core samples. Taking the example shown in Figure 1, gray-level co-occurrence matrices were calculated in different directions, as shown in Table 3. Feature parameter values obtained in each direction were averaged, and these averages were used as the final feature parameters for neural network training. This approach, leveraging the characteristics of gray-level co-occurrence matrices, involves feature extraction and averaging operations in multiple directions, aiming to comprehensively capture the texture information of core sample images and enhance the performance of neural networks in core image classification tasks.

Using the gray-level co-occurrence matrix, features were extracted from the core images in the training set. These features were then employed to train a neural network model, setting the input layer to 6 and the output layer to 6 based on the input type. The model was trained with varying numbers of iterations, observing changes in recognition rates. The optimal number of training iterations was determined. Similar to the color moment approach, the same neural network model was employed. Ultimately, an accuracy of approximately 80% was achieved. As depicted in Figure 7.

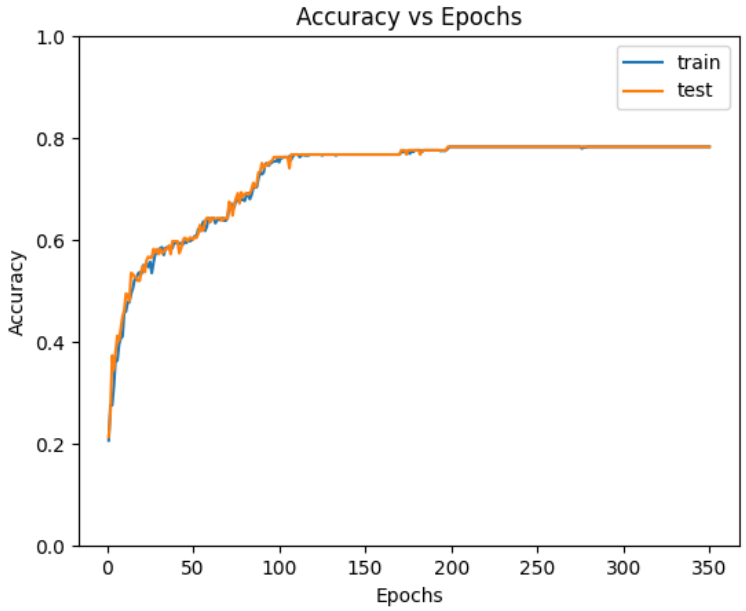

Figure 7. Accuracy under Gray-Level Co-occurrence Matrix Features

3.4. Color Moments and GLCM Fusion Recognition

By extracting color and texture features from core images and utilizing the constructed neural network for recognition, it was observed that individual features exhibited relatively lower accuracy in lithology recognition. Faced with this result, it is proposed to consider multi-feature fusion of color and texture features in core image analysis to improve lithology recognition accuracy. Since feature fusion may lead to high-dimensional data, posing issues of data redundancy, Principal Component Analysis (PCA) is introduced to perform dimensionality reduction on the data. In the process of multi-feature fusion, the sharp increase in data dimensions may affect the model's performance and computational efficiency. Therefore, PCA is employed to reduce the dimensionality of the data, retaining essential feature information while reducing the data's dimensionality. The reduced-dimensional data is then used for the training of the neural network model, and the recognition process is illustrated in Figure 8.

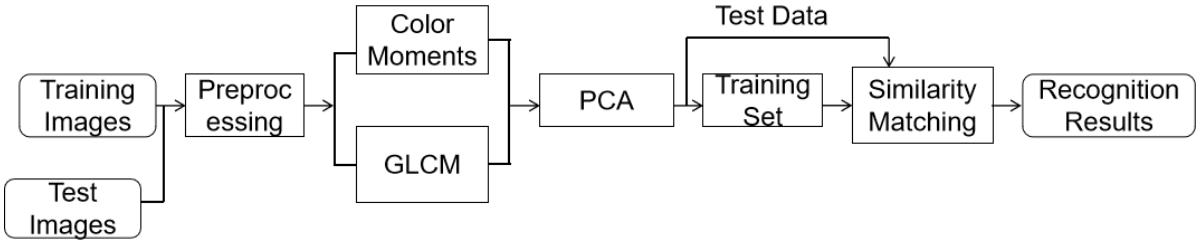

Figure 8. Lithology Recognition Workflow

According to the recognition workflow, it is evident that the fusion of two individual features is performed for multi-feature recognition. Due to the change in input types, the neural network's input layer also becomes 15. The recognition rate after the fusion of multiple features is obtained using the same method, as shown in Figure 9. It is clearly visible from the graph that the accuracy obtained by fusing two features is higher than that of single-feature recognition, with an accuracy of approximately 85%.

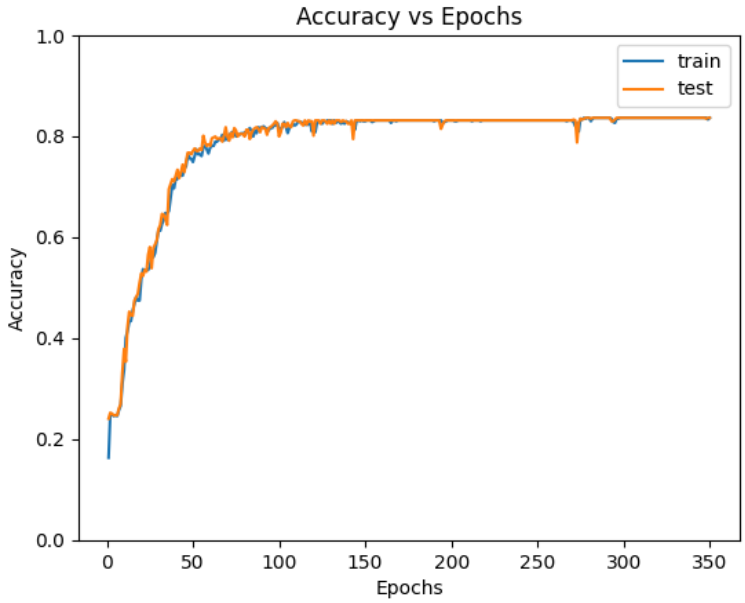

Figure 9. Accuracy under Multi-feature Fusion

4. CONCLUSION

Through the use of the same neural network model, training was conducted using three features separately - color moments, gray-level co-occurrence matrix (GLCM), and the fusion of color moments and GLCM. By comparing the obtained accuracy graphs, it is clearly observed that the accuracy is significantly higher in the case of multi-feature fusion. This indicates that recognizing lithology in cores using multi-feature fusion is more precise. It can analyze both color and texture features, leading to more accurate lithology recognition. This method greatly improves the accuracy of lithology recognition in core images.

REFERENCES

[1] Deng Wenjing, Zhou Wu, Cai Xiaoshu. Multidimensional Feature KFCM Clustering Segmentation Algorithm for Core Particle Color Images[J]. China Powder Science and Technology, 2019, 25(06): 12-18.

[2] Wu Xiaohong, Wang Zhengyong, Luo Daisheng. A Rock Image Segmentation Method Combining Watershed and ISODATA[J]. Computer Application, 2008(01): 214-215+219.

[3] Chen Jiajun. Analysis of Basic Structure and Depositional Lithostructure of Geological Bodies[J]. Nonferrous Metal Engineering, 2023, 13(06): 149.

[4] Zhang Chi, Pan Mao, Hu Shuiqing, et al. Machine Learning Lithology Identification Method Incorporating Vertical Information of Reservoirs[J]. Geological Science and Technology Bulletin, 2023, 42(03): 289-299.

[5] Meng X. Sedimentary Structure Characteristics and Depositional Facies of Paleogene Es4 in Dongying Sag, Jiyang Depression, Bohai Bay Basin, China[C]. Earth and Environmental Science, 2020, 474(4).

[6] Ren Yili, Liang Jia, Yang Yanzi, Zhang Xiaoyu. Intelligent Identification Technology of Lithology Considering Core Images and Well Logging Curves[J]. Information Systems Engineering, 2021(03): 78-80.

[7] Bai Lin, Yao Yu, Li Shuangtao, et al. Mineral Composition Analysis of Rock Images Based on Deep Learning Feature Extraction[J]. China Mining, 2018, 27(07): 178-182.

[8] Chen Hao, Mu Longxin, Huang Jixin, et al. Quantitative Characterization of Mudstone Lamination Based on Mathematical Morphology Image Processing: A Case Study of the McKay River Oil Sands Block in Canada[J]. Science Technology and Engineering, 2018, 18(26): 77-83.

[9] Zhu Qiangjun, Wu Xiaohong, Teng Qizhi, et al. Layer Characteristic Extraction of Core Images Based on Fuzzy Algorithm[J]. Electronic Measurement Technology, 2008, No.167(03): 58-60.

[10] Zhang B, Chen S, Xiao Y, et al. Vision-based Sedimentary Structure Identification of Core Images using Transfer Learning and Convolutional Neural Network Approach[C]. SPE/AAPG/SEG Unconventional Resources Technology Conference. URTEC, 2021.

[11] Li Jiahang, Li Wei, Liu Xiangjun, et al. Method and Application of Shale Lamination Identification in Transitional Marine-Land Facies Based on Rock Thin Section Images[J]. Special Oil & Gas Reservoirs, 2023, 30(04): 44-53.

[12] Borazjani O, Ghiasi-Freez J, Hatampour A. Two intelligent pattern recognition models for automatic identification of textural and pore space characteristics of the carbonate reservoir rocks using thin section images[J]. Journal of Natural Gas Science and Engineering, 2016, 35:944-955.

[13] Peng Yue, Zhang Manlang, Li Mingqiu, et al. A New Method for Quantitative Evaluation of Fracture Development Based on Image Recognition Technology: A Case Study of Xushen Gas Reservoir in Anyue Gas Field[J]. Unconventional Oil & Gas, 2024, 11(01): 12-21.

[14] Hu Bo, Pu Jun, Gou Feifei. Quantitative Characterization of Microscopic Pore Throat Structure in Tight Sandstone Based on Digital Core[J]. Petroleum Geology and Recovery Efficiency, 2022, 29(03): 102-112.

[15] Yu Xiaolu, Ye Kai, Du Chongjiao, et al. Recognition of Microscopic Images of Carbonate Rock Biominerals Based on Convolutional Neural Network[J]. Petroleum Geology Laboratory, 2021, 43(05): 880-885+895.

[16] Qin Rong, Liu Liyuan, Wang Jingjing, et al. Application of XRF Scanning in the Study of Annual Lamination of Lakes: A Case Study of Xinluhai in the Southeastern Margin of the Qinghai-Tibet Plateau[J]. Journal of Lake Sciences, 2022, 34(05): 1723-1734.

[17] Heather Dunlop, David R. Thompson, David Wettergreen. Multi-scale Features for Detection and Segmentation of Rocks in Mars Images[J]. The Robotics Institute Carnegie Mellon University 2007.

[18] Zhang Ye, Li Mingchao, Han Shuai. Rock Lithology Automatic Identification and Classification Method Based on Deep Learning of Rock Images[J]. Acta Petrologica Sinica, 2018, 34(02): 333-342.

[19] Liu Litin. Application Research of Deep Belief Network in Rock Thin Section Image Processing[D]. Xi'an Shiyou University, 2017.

[20] Song Wenguang, Xu Hao, Wang Hao, et al. Intelligent Identification Method of Rock Thin Section Lithology Based on Generative Adversarial Network[J]. Journal of Yangtze University (Natural Science Edition), 2022, 19(02): 39-46.

[21] Zhang Zhongya. Study on Sandstone Thin Section Image Segmentation and Recognition[D]. University of Science and Technology of China, 2020.

[22] Ma Zedong, Ma Lei, Li Ke, et al. Multi-Scale Lithology Identification Based on Deep Learning of Rock Images[J]. Geological Science and Technology Bulletin: 1-7 [2022-10-15].